Technical Notes

TECHNICAL NOTES are short manuscripts describing new developments or important results of a preliminary nature. These Notes cannot exceed 6 manuscript pages and 3 figures; a page of text may be substituted for a figure and vice versa. After informal review by the editors, they may be published within a few months of the date of receipt. Style requirements are the same as for regular contributions (see inside back cover).

Numerical Viscous Flow Analysis Around a High-Speed Train with Crosswind Effects

Warn-Gyu Park* and Young-Rae Jung†
Pusan National University, Pusan 609-735, Republic of Korea
and
Seong-Do Ha‡
Korea Institute of Machinery and Materials, Daejeon 305-600, Republic of Korea

Introduction

RECENTLY, a high-speed train having the maximum Mach number of 0.25–0.3 has been developed in several countries to satisfy demands for new systems of fast and comfortable mass transportation. To predict unsteady aerodynamic loads, performances, and acoustic noise level at this high speed, the accurate simulation of the flowfield is needed. The objective of the present work is to apply the iterative time-marching scheme[1] to the incompressible turbulent flow around a high-speed train with crosswind effects. Even though the crosswind may significantly affect the longitudinal and lateral stabilities of the train, the details of flow properties of the crosswind are not well understood.

Numerical Formulation

The three-dimensional incompressible Navier–Stokes equations may be written as follows:

$$\frac{\partial \hat{q}}{\partial \tau} + \frac{\partial}{\partial \xi}(\hat{E} - \hat{E}_\nu) + \frac{\partial}{\partial \eta}(\hat{F} - \hat{F}_\nu) + \frac{\partial}{\partial \zeta}(\hat{G} - \hat{G}_\nu) = 0 \qquad (1)$$

where $\hat{E}$, $\hat{F}$, and $\hat{G}$ denote the convective flux terms and $\hat{E}_\nu$, $\hat{F}_\nu$, and $\hat{G}_\nu$ denote the viscous terms. Let us consider the momentum equation first. Because the momentum equation is a parabolic partial differential equation, it can be solved using a time-marching and Newton iteration scheme as follows:

$$(1/\Delta\tau)(\bar{q}^{n+1,k+1} - \bar{q}^n) + (\delta_\xi \bar{E} + \delta_\eta \bar{F} + \delta_\zeta \bar{G})^{n+1,k+1}$$
$$= (\delta_\xi \bar{E}_\nu + \delta_\eta \bar{F}_\nu + \delta_\zeta \bar{G}_\nu)^{n+1,k+1} \qquad (2)$$

where the barred quantities are the same quantities of Eq. (1) excluding the continuity equation. Following a local linearization of $\bar{E}, \bar{F}, \bar{G}, \bar{E}_\nu, \bar{F}_\nu$, and $\bar{G}_\nu$ about the $n + 1$ time level and at the k iteration level,

$$\left(\frac{I}{\Delta\tau} + \frac{\partial A}{\partial \xi} + \frac{\partial B}{\partial \eta} + \frac{\partial C}{\partial \zeta}\right)\Delta\bar{q} = \omega \bar{R}^{n+1,k} \qquad (3)$$

where ω is a relaxation factor. The terms A, B, and C are the Jacobian matrices of the flux vectors $\bar{E}-\bar{E}_\nu$, $\bar{F}-\bar{F}_\nu$, and $\bar{G}-\bar{G}_\nu$, respectively. The term $\bar{R}^{n+1,k}$ is the residual vector, defined as

$$\bar{R}^{n+1,k} = -\frac{\bar{q}^{n+1,k+1} - \bar{q}^n}{\Delta\tau} - (\delta_\xi \bar{E} + \delta_\eta \bar{F} + \delta_\zeta \bar{G})^{n+1,k}$$
$$+ (\delta_\xi \bar{E}_\nu + \delta_\eta \bar{F}_\nu + \delta_\zeta \bar{G}_\nu)^{n+1,k} \qquad (4)$$

To capture the strong viscous flow effects of a vortex pair in the wake and flow separation at high-Reynolds-number flows, the k–ε model[2] was implemented. Next, let us consider the continuity equation. To solve incompressible flow problems efficiently, we need a relationship coupling change in the velocity field with changes in the pressure field while satisfying the divergence-free constraint. The MAC (Marker-and-Cell) approach[3] is used in the present study:

$$\Delta(p/J) = -\beta[\delta_\xi\{(U - \xi_t)/J\} + \delta_\eta\{(V - \eta_t)/J\}$$
$$+ \delta_\zeta\{(W - \zeta_t)/J\}]^{n+1,k} \qquad (5)$$

where β is a relaxation factor. The spatial derivatives of convective flux terms are differenced by using the QUICK scheme[4] to reduce unphysical oscillations, and the spatial derivatives of viscous terms and continuity equation are differenced with central differencing. The fourth-order artificial damping term is added to stabilize the present procedure. Combining Eqs. (3) and (5), a system of simultaneous equation for the quantity $\Delta\hat{q}$ may be formally written as

$$[M]\{\Delta\hat{q}\} = \{R\} \qquad (6)$$

Here, because the right-hand side of Eq. (6) is the governing equation, as long as $\{\Delta\hat{q}\}$ is driven to zero, the discretized forms of unsteady Navier–Stokes equations are exactly satisfied at physical time level $n + 1$. Then the solution is independent of ω and any approximations made in the construction of A, B, and C of Eq. (3) and is also independent of β of Eq. (5). Although the matrix $[M]$ is a sparse and banded block matrix, direct inversion of this matrix requires a huge number of arithmetic operations. A common strategy is to approximate the matrix $[M]$ by another, easily inverted matrix $[N]$. In this study, matrix $[N]$ contains only the diagonal contributions of matrix $[M]$, and Eq. (6) becomes an explicit form that is more easily tailored for efficient execution on the current generation of vector or massively parallel computer architectures than an implicit form.

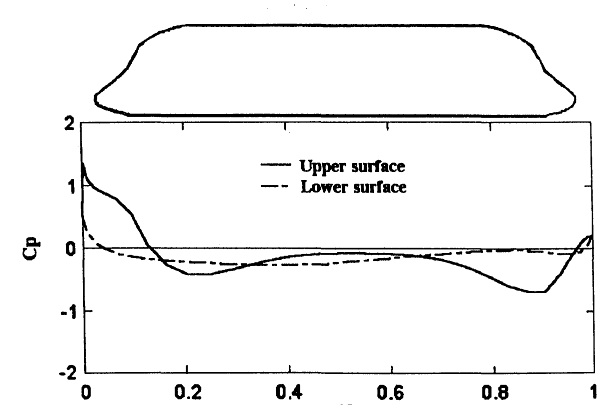

Fig. 1 Surface pressure distribution in the symmetry plane at zero yaw angle.

Received Sept. 3, 1996; revision received Nov. 12, 1997; accepted for publication Nov. 17, 1997.

*Assistant Professor, School of Mechanical Engineering. Member AIAA.
†Graduate Research Assistant, School of Mechanical Engineering.
‡Senior Research Engineer, New Transport Technology Department.

Results and Discussion

The present iterative time-marching procedure has been applied to the flow around the high-speed train with a single car at a Reynolds number of 1.26×10^8 and at four yaw angles of 0, 9.2, 16.7, and 45 deg. The surface pressure distribution in the symmetry plane at zero yaw angle is shown in Fig. 1. Figure 2 shows the streamwise pressure distribution in the three planes, i.e., along the windward side wall, the midplane, and the leeward side wall at yaw angles of 9.2, 16.7, and 45 deg. The locations of plane a'–a', b'–b', and c'–c' are shown in Fig. 3d. Figure 3 shows the cross-sectional surface pressure distributions in the five cross-sectional planes. The positions of numbers 1 ~ 30 are chosen as starting from the center of the upper surface to the center of the lower surface. Because the position from 10 to 20 denotes the side wall, the pressure difference at the windward and leeward sides induces the side force and yawing moment. The aerodynamic coefficients as a function of yaw angle

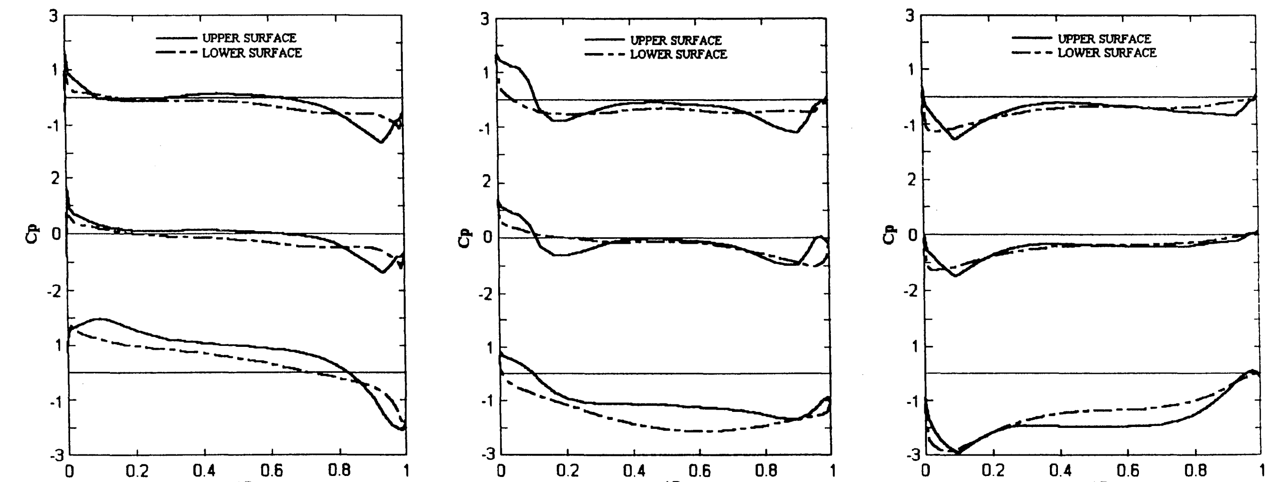

a) Along windward side wall, A'–A', $\theta = 9.2$ deg

b) Along midplane plane, B'–B', $\theta = 16.7$ deg

c) Along leeward side wall, C'–C', $\theta = 45$ deg

Fig. 2 Surface pressure distribution along the three streamwise planes at each yaw angle.

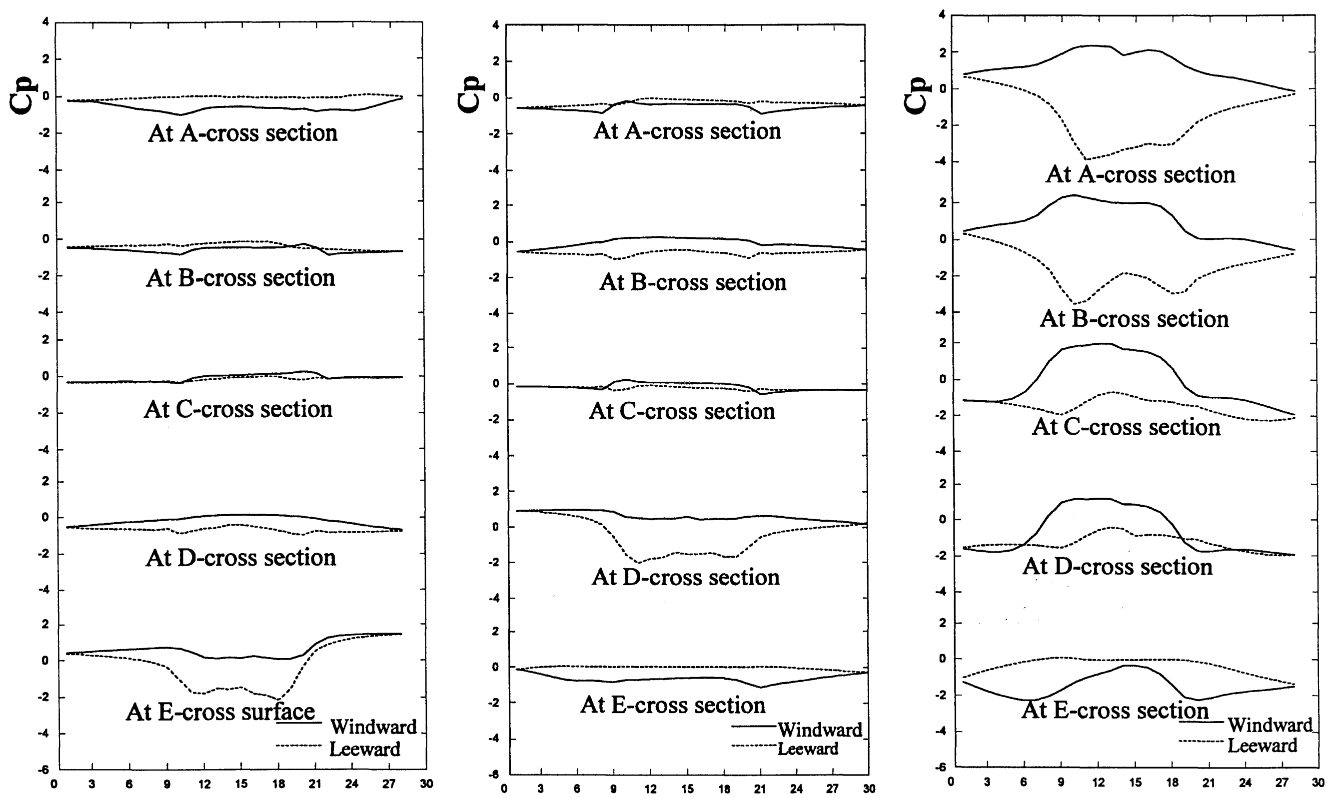

a) $\theta = 9.2$ deg

b) $\theta = 16.7$ deg

c) $\theta = 45$ deg

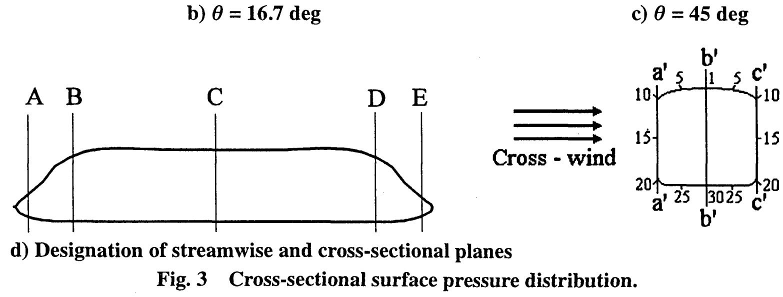

d) Designation of streamwise and cross-sectional planes

Fig. 3 Cross-sectional surface pressure distribution.

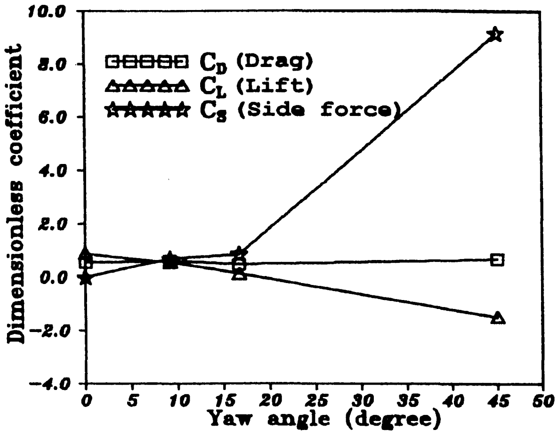

a) Aerodynamic forces

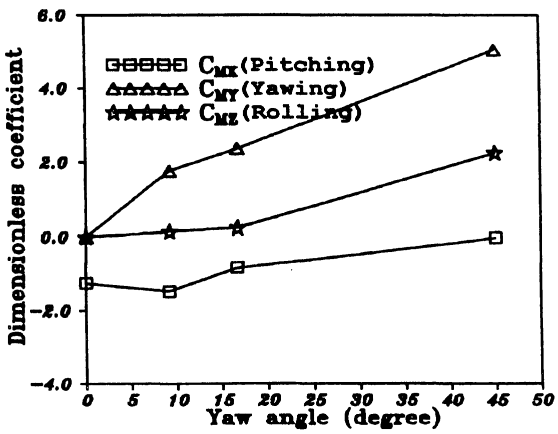

b) Aerodynamic moments

Fig. 4 Aerodynamic coefficients as a function of yaw angle.

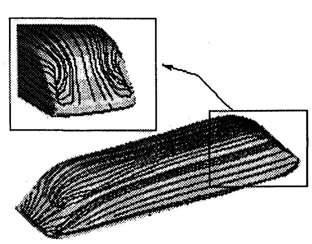

a) Yaw angle of 0 deg

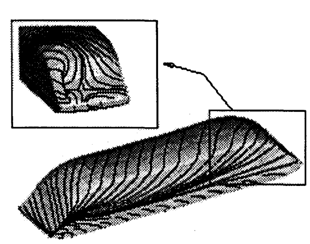

b) Yaw angle of 45 deg

Fig. 5 Limiting streamlines on the surface.

are shown in Fig. 4. The lift, drag, and side force coefficients are based on the frontal area. The pitching, yawing, and rolling moment coefficients about the center of gravity are based on the height of the train. Figure 5 shows the limiting streamlines on the surface at 0- and 45-deg yaw angles. Figure 6a shows streamlines and crossflow vectors just behind the train body at yaw angle of 0 deg. The generation of a vortex pair is evident. Figure 6b shows streamlines and vectors at the yaw angle of 9.2 deg. The vortex on the windward side becomes stronger than that on the leeward side due to the crosswind effects because the rotative motion of the crossflow components of the leeward side vortex may cancel with the crossflow of the freestream. Figure 6d shows a yaw angle of 45 deg, and the vortex is not shown in both sides due to strong crosswind effects.

Concluding Remarks

The iterative time-marching procedure for the solution of three-dimensional incompressible turbulent flows has been successfully applied to the flows around a high-speed train with crosswind effects.

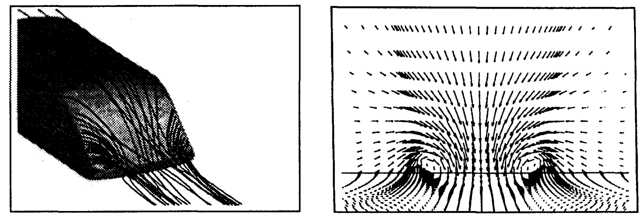

a) Yaw angle of 0 deg

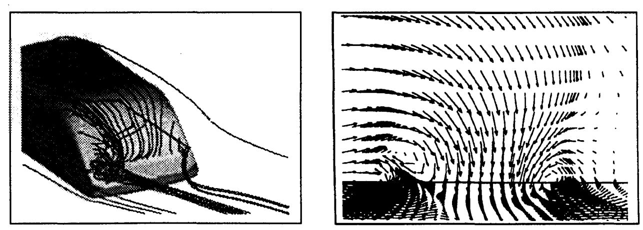

b) Yaw angle of 9.2 deg

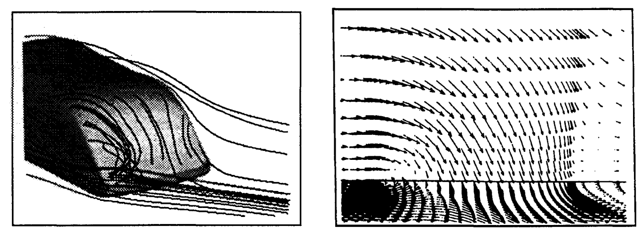

c) Yaw angle of 16.7 deg

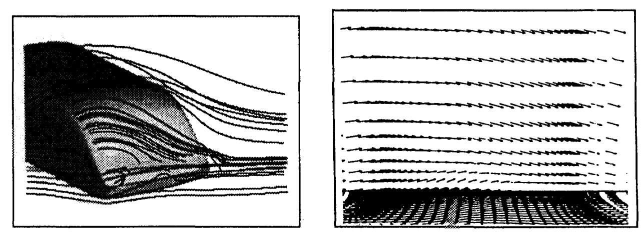

d) Yaw angle of 45 deg

Fig. 6 Streamlines and velocity vectors just behind the train body.

The governing equations are implicitly discretized with a backward scheme for the time derivatives, the QUICK scheme for convective terms, and the central difference scheme for viscous terms. The Marker-and-Cell concept was used to efficiently solve the continuity equation. The turbulent flows around a high-speed train with the crosswind effects of four yaw angles of 0, 9.2, 16.7, and 45 deg are well simulated.

Acknowledgments

The authors would like to acknowledge the financial support of the Korea Science and Engineering Foundation and the Korea Institute of Machinery and Materials.

References

[1]Park, W. G., and Sankar, L. N., "A Technique for the Prediction of Unsteady Incompressible Viscous Flows," AIAA Paper 93-3006, July 1993.

[2]Jones, W. P., and Launder, B. E., "The Prediction of Laminarization with a 2-Equation Model of Turbulence," *International Journal of Heat and Mass Transfer*, Vol. 15, Feb. 1972, pp. 301–314.

[3]Viecelli, J. A., "A Method for Including Arbitrary External Boundaries in the MAC Incompressible Fluid Computing Technique," *Journal of Computational Physics*, Vol. 4, 1969, pp. 543–551.

[4]Leonard, B. P., "A Stable and Accurate Convective Modelling Procedure Based on Quadratic Upstream Interpolation," *Computer Methods in Applied Mechanics and Engineering*, Vol. 19, 1979, pp. 59–98.

J. Kallinderis
Associate Editor